1994PASJ...46L.125K

PASJ: Publ. Astron. Soc. Japan **46**, L125–L129 (1994)

ASCA Observations of Hard X-Ray Emission from the Rho Ophiuchi Dark Cloud

Katsuji KOYAMA, Yoshitomo MAEDA, Masanobu OZAKI, and Shiro UENO
Department of Physics, Faculty of Sciences, Kyoto University, Sakyo-ku, Kyoto 606-01

Yuichi KAMATA and Yuzuru TAWARA
Department of Astrophysics, Nagoya University, Chikusa-ku, Nagoya 464-01

Stephen SKINNER
Institute of Space and Astronautical Science, 3-1-1 Yoshinodai, Sagamihara, Kanagawa 229
and
Shigeo YAMAUCHI
College of Humanities and Social Sciences, Iwate University, 3-18-34 Ueda, Morioka, Iwate 020

(Received 1994 January 26; accepted 1994 April 1)

Abstract

ASCA obtained broad-band (0.8–12 keV) images and spectra of the central region of the Rho Ophiuchi dark cloud in 1993 August. The 38-ks observation detected at least eleven sources (S/N $\geq$ 3), including the X-ray bright pre–main-sequence star DoAr 21 and embedded infrared sources with no optical counterparts. Hard X-rays up to $\approx$ 8 keV were detected from DoAr 21 (whose light curve shows no evidence for variability) and from a flaring source lying in a region of high visual extinction. Thermal spectral fits for the brightest source give $kT \approx 2$ keV and hydrogen column densities $N_{\rm H} \approx 10^{22}{\rm cm}^{-2}$. The spectrum of a region in the center of the field where no discrete sources were detected shows hard, heavily absorbed emission that is most likely the integrated contribution of a number of deeply embedded young stars below the detection limit.

Key words: ISM: clouds — Stars: flare — Stars: pre–main-sequence — X-rays: sources

1. Introduction

The Rho Ophiuchi dark cloud is a nearby ($\approx$ 140 pc) star-forming region that is rich in low-mass pre–main-sequence (PMS) objects including visible T Tauri stars and embedded infrared sources. Einstein Observatory revealed that many of these young stars emit soft X-rays with apparent luminosities in the 0.5–4 keV energy band of $(0.5\text{–}25) \times 10^{30}$ erg s^{-1} (Montmerle et al. 1983). The intensity of the X-ray emission can exceed that of the sun by factors of $\sim 10^4$, and is often variable on short timescales of $\leq$ 1d. The X-rays are thought to arise in magnetically confined hot plasma ($T \sim 10^7$ K) near the stellar surface, and the short-term variability has been attributed to scaled-up solar-like flares (cf. the review by Feigelson et al. 1991).

Einstein Observatory as well as the newer ROSAT observatory were sensitive only to softer X-rays in the energy bands below $\approx$ 3–4 keV. Consequently, there has been little opportunity to study the X-ray properties of young stars at higher energies. However, the Ginga satellite provided some evidence that PMS stars emit X-rays at energies well above the Einstein 4 keV cutoff. Ginga obtained a composite X-ray spectrum of a $1^\circ \times 2^\circ$ region in the center of the Rho Ophiuchi cloud in 1990 March covering the 1.5–16 keV energy band (Koyama et al. 1992). A best fit of the composite spectrum was obtained with an optically thin thermal plasma model of temperature $kT = 4.1 \pm 0.2$ keV plus an emission line from He-like iron at 6.6 keV. This temperature is a factor of two higher than previously obtained for PMS stars. Furthermore, Ginga detected a decaying flare with an inferred flare temperature of at least 4 keV, although the source responsible for the flare could not be identified since Ginga lacked imaging capability.

ASCA provides for the first time the capabilities needed to conduct detailed studies of hard X-ray emission from individual PMS stars. These capabilities include broad-band imaging and high-resolution spectroscopy in the range 0.5–12 keV and an on-axis spatial resolution of $\approx 1'$, which is often sufficient to identify optical or infrared counterparts. We illustrate these unique capabilities here by presenting the first results of a 38-ks observation of the central region of the Rho Ophiuchi dark cloud. These observations reveal hard X-rays at energies up to $\approx$ 8 keV from visible objects such as the active T Tauri

© Astronomical Society of Japan • Provided by the NASA Astrophysics Data System

1994PASJ...46L.125K

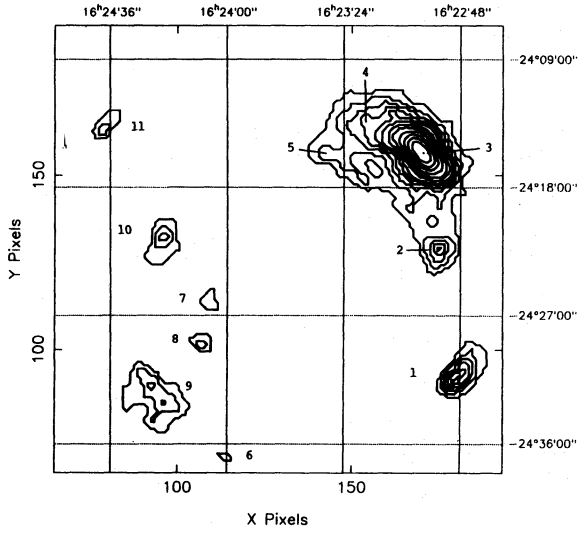

Fig. 1. Smoothed broad-band (0.8–12 keV) GIS 2 image of the Rho Ophiuchi central region. Lowest contour is S/N = 2.5. The FWHM of the convolved telescope+GIS PSF is $\approx 1'.2$ at 2 keV. Coordinate overlay (1950.0) is uncertain by $\approx 1'$. Source numbers refer to table 1.

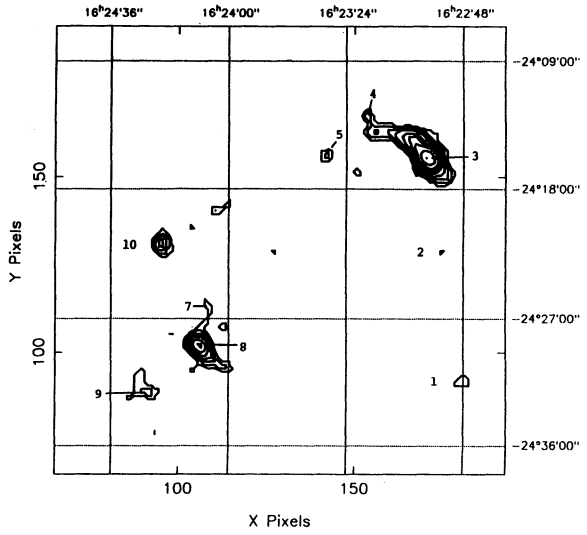

Fig. 2. Same as figure 1 except image is restricted to the hard energy band 5–10 keV. Lowest contour is S/N = 3.4. The FWHM of the convolved telescope+GIS PSF is $\approx 0'.8$ at 5.9 keV.

star DoAr 21 and from embedded infrared sources with no optical counterparts.

2. Observations

ASCA observed the Rho Ophiuchi dark cloud for 37868 s on 1993 August 20 from 02:19–22:17 UT. The pointing was centered at RA(2000) = 16h 26m 44.5s and DEC(2000) = $-24°28'48''.0$. All four instruments were operating simultaneously, including two Solid-State Imaging Spectrometers (SIS 0, SIS 1) and two Gas Imaging Spectrometers (GIS 2, GIS 3). The field of view of each SIS is $\approx 22' \times 22'$ (4-CCD mode), compared to a circular field-of-view for each GIS of usable diameter $\approx 40'$. The SIS and GIS passbands are 0.4–10 keV and 0.8–12 keV respectively, with corresponding energy resolutions at 5.9 keV of 2% and 8%. The GIS point spread function (PSF) scales with energy E (keV) as FWHM=$0.5\sqrt{5.9/E}$ arcmin. Convolving the GIS and telescope PSFs gives a spatial resolution of $\approx 1'.2$ at 2 keV and $\approx 0'.8$ at 5.9 keV. The SIS spatial resolution is better than $1'$. Further details on the spacecraft and instrumentation are given in Tanaka et al. (1994), Serlemitsos et al. (1994), Burke et al. (1991), and Ohashi et al. (1991). Data were post-processed to correct for spatial and gain nonlinearities, remove hot and flickering CCD pixels, and reject data taken at low earth elevation angles $\leq 15°$ for GIS, $\leq 25°$ for SIS).

3. Results

Figures 1 and 2 show the broad-band (0.8–12 keV) and hard-band (5–12 keV) GIS 2 images. The hard image provides better spatial resolution, but at lower S/N. Table 1 lists the eleven GIS detections with S/N ≥ 3. All of these detections are confirmed in the SIS images, except source 6 which lies outside the SIS field-of-view and is thus classified as a possible detection. The weak source $\approx 4'$ northwest of source 10 in figure 2 is not confirmed in the other cameras and is thus not listed as a detection.

The ASCA positions are uncertain by $\approx 1'$ in both RA and DEC, primarily because of imprecise knowledge of the telescope boresite alignment early in the mission. However, we were able to register the ASCA SIS 1 image with a ROSAT PSPC image taken in 1991 by shifting the SIS 1 image 1.0 s in RA and $19''$ in DEC. This aligned sources 1, 2, 3, and 9 with corresponding ROSAT sources, allowing us to identify source 3 from its ROSAT coordinates as the active PMS star DoAr 21. The known offset was then used to identify counterparts to several of the other ASCA sources (table 1). Due to crowded infrared fields, several possible counterparts exist for sources 7, 8, and 10.

Sources 2, 8, and 10 are clearly variable, as indicated by χ^2 values for fits of a constant source to the binned

© Astronomical Society of Japan • Provided by the NASA Astrophysics Data System

1994PASJ...46L.125K

Table 1. ASCA X-ray detections in Rho Ophiuchi (GIS detector, S/N $\geq$ 3).

No	Einstein identification	Optical/IR identification	X-ray position RA (1950) (h m s)	X-ray position DEC (1950) (° ′ ″)	Total counts (cts)	log L_X (ergs s $^{-1}$)	Hardness ratio	Variation probability
(1)	(2)	(3)	(4)	(5)	(6)	(7)	(8)	(9)
1	ROX-4	VSS 23	16 22 50	−24 31 11	749	30.13 (31.4)	0.1	≤70%
2	ROX-7	GSS 20	16 22 57	−24 22 52	563	30.11 (31.1)	0.2	≥99%
3	ROX-8	DoAr 21	16 23 02	−24 16 17	5382	30.83 (32.2)	0.1	≤1%
4	ROX-11?	...	16 23 16	−24 14 45	170	29.7:	...	...
5	ROX-14	...	16 23 33	−24 15 41	220	29.7:	...	...
6	ROX-C13?	DoAr 29	16 24 00	−24 38 22	267	29.80	0.1	≥80%
7	...	GY 211,220; WL 10	16 24 07	−24 26 36	142	29.5:	...	...
8	...	GY 214,226; WL 15	16 24 08	−24 29 27	230	29.7:	...	≥99%
9	ROX-21	SR 12	16 24 19	−24 33 58	530	30.07 (30.2)	0.2	≥70%
10	...	GY 254,256,257; WL 3,6	16 24 20	−24 22 14	409	29.96	0.9	≥99%
11	ROX-29	DoAr 34	16 24 37	−24 15 01	227	29.72 (29.8)	−0.6	≤40%

Columns: (1) Refers to figure 1 (2) Refers to tables 1 and 2 of Montmerle et al. (1983) (3) GSS = Grasdalen et al. (1973), GY = Greene Young (1992), HB = Herbig Bell (1988), SR = Struve and Rudkjøbing (1949), VSS = Vrba et al. (1976), WL = Wilking and Lada (1983) (4)–(5) ASCA positions are uncertain by $\approx 1'$ in each coordinate. (6) Total GIS 2 counts in 37868 s, background subtracted. (7) Observed luminosity in 0.8–10 keV band, assuming $d = 140$ pc (de Geus, Burton 1991), followed in parentheses by extinction corrected value using A_V from Bouvier and Appenzeller (1992). Typical internal uncertainties are 0.3 dex. A colon denotes L_X was obtained from a simulated thermal spectrum with $kT = 2$ keV and log $N_H = 22$ cm^{-2} normalized to observed count rate, rather than by fitting the GIS spectrum. (8) Hardness ratio = [cts (2–12 keV) − cts (0.8–2 keV)] / cts (0.8–12 keV). (9) Variability probability from χ^2 of best fit of a constant count rate source to binned light curve.

Notes on Sources:

(1) Thermal spectral fits give $kT = 2.0$ keV and log $N_H = 22.0$ cm^{-2}.

(2) X-ray flare. The quoted L_X is the average over the entire observation. Log L_X (pre-flare) = 29.8 ergs s^{-1} and log L_X (flare) = 30.5 ergs s^{-1}. Thermal spectral fits give log $N_H = 22.0$ cm^{-2} with $kT = 1.5$ keV (pre-flare) and $kT = 2.3$ keV (flare).

(3) =HB 637. Two-temperature RS fits give $kT_1 = 0.4$–0.6 keV, $kT_2 = 1.55$–2.1 keV, and log $N_H = 22.3$ cm^{-2}.

(4) Counts are from SIS 0 and are uncertain by $\approx 50\%$ due to proximity of DoAr 21.

(6) Einstein and optical id uncertain. Coordinates are from GIS only; source is out of SIS field. Classified as possible detection.

(7) IR identification uncertain (dense field).

(8) IR identification uncertain (dense field). X-ray flare. Quoted L_X is average over entire observation. Hard source.

(9) =HB 263. Double star (HB). Double X-ray peak suggests multiple source. No acceptable spectral fit obtained.

(10) IR identification uncertain (dense field). Hard spectrum shows heavy absorption and possible Fe emission line at ≈ 6.9 keV. Thermal fits give $kT \approx 2.2$ keV and log $N_H \approx 22.6$ cm^{-2}, with large uncertainties.

(11) =HB 264. Soft spectrum with $kT \approx 0.8$ keV and log $N_H \leq 21.6$ cm^{-2}.

light curves (table 1). The variability in sources 2 and 8 is flare-like. After emerging from earth occultation with ≈ 2.4 hours remaining in the observation, the count rate of source 2 had risen by a factor of 6. It decreased steadily but was still above its pre-event level at the end of the observation, with an e-folding time of ≈ 2.5 hours. The event in source 8 was similar, with a factor of 5–6 increase in the count rate, a rise time ≤ 1.5 hours, and decay timescale of ≈ 3 hours. Surprisingly, the brightest detection DoAr 21 shows no significant variability down to time bins of 4 min.

The hardness ratios (HR) in table 1 show that the variable source 10 is the hardest (HR = +0.9). Hard photons with energies up to ≈ 8 keV were also detected from DoAr 21 and flaring source 8. DoAr 34 is considerably softer (HR = −0.6), indicating that it lies near the front of the cloud. This is supported by its low visual extinction of $A_V = 0.2$ magnitudes (Bouvier, Appenzeller 1992).

Fits of the GIS spectra of the brighter sources using single-temperature Raymond-Smith (RS) and thermal bremsstrahlung (TB) models typically give $kT \approx 2$ keV and column densities $N_H \approx 10^{22}$ cm^{-2} (table 1). In most cases, the TB model gives slightly lower residuals than a single-temperature RS model. An exception is the soft source DoAr 34, for which the RS fit is supe-

© Astronomical Society of Japan • Provided by the NASA Astrophysics Data System

1994PASJ...46L.125K

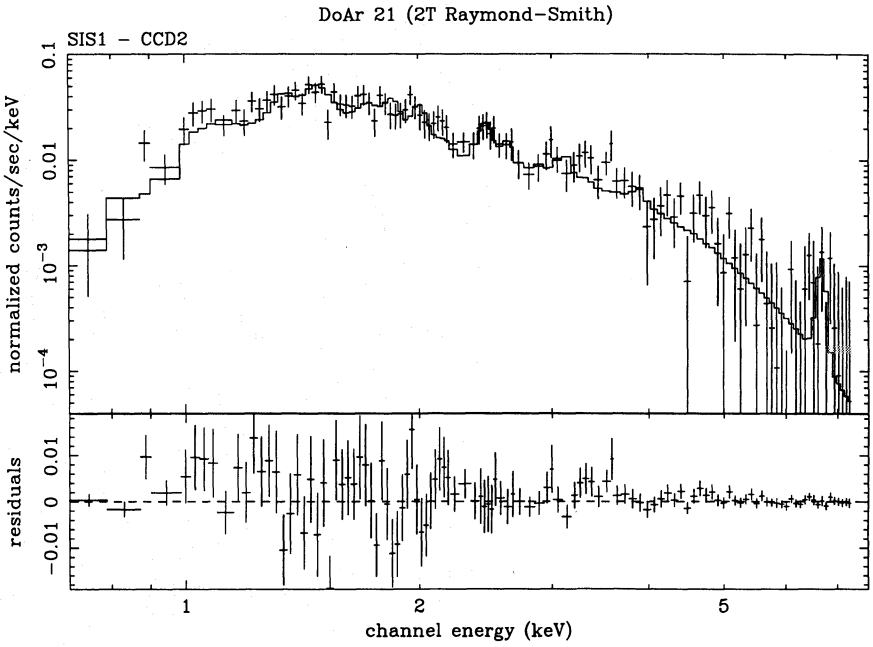

Fig. 3. Background-subtracted SIS 1 spectrum of DoAr 21, corrected for off-axis response. The circular region of 1′.3 radius used to extract the spectrum encloses 2440 counts (source + background). Solid line is two-temperature Raymond-Smith fit with $kT_1 = 0.4$ keV, $kT_2 = 1.6$ keV, $\log N_{\rm H} = 22.29{\rm cm}^{-2}$, and reduced $\chi^2 = 0.996$ over 234 energy channels. Weak line emission at 2.46 keV is S XIV/XV. The residual just below 2.2 keV is an Au M feature from the X-ray telescope.

rior. No acceptable fit was obtained for source 9, and its double-peaked structure in both the GIS and SIS images suggests a multiple source. Generally we were not able to check for improvement in the RS fit by adding a second cool plasma component (≤ 1 keV) because of the low counts per source and the strong low-energy absorption. However, for DoAr 21 there were sufficient counts to try a two-component RS fit, and a definite improvement was seen by adding a cool component at ≈ 0.5 keV (section 4). Thus, only for this bright source are we able to confirm the improvement using two-temperature RS fits that has been found in other T Tauri stars (Strom, Strom 1994).

4. Discussion

Figure 2 is the first hard X-ray image (≥ 5 keV) ever obtained of a nearby star-forming region, and provides a wealth of new information. It reveals a discrete hard component that is due to both visible T Tauri stars such as DoAr 21, which emits ≈ 30 % of its flux above 4 keV, and embedded objects with no optical counterparts such as the variable sources 8 and 10. Thus, hard X-ray emission is not restricted to the optical sample, and may be present before a young star reaches the birthline.

But the discrete emission is only part of the picture, and we have also detected a hard *unresolved* component. Several GIS spectra were extracted from regions between sources 2 and 10, taking care not to include any of the discrete detections. Background was subtracted from a region between sources 1 and 6. These spectra show hard, heavily absorbed emission with a weak Fe line at 6.9 ± 0.3 keV. The temperature is uncertain and depends somewhat on the region sampled, but Raymond-Smith fits give values in the range 3–7 keV and $N_{\rm H} \approx 3$–4×10^{22} cm^{-2}. This range of $N_{\rm H}$ implies a visual extinction $A_V \approx 13$–18 magnitudes (Gorenstein 1975), and we thus postulate that the hard excess is the integrated contribution of a number of deeply embedded young stars below our detection limit. These objects undoubtedly have different plasma temperatures, which would explain the inability to obtain an accurate single-temperature fit. The measured luminosity in circular regions of radius 5′ located between sources 2 and 10 is $\log L_{\rm X} \approx 30.2$ erg s^{-1}(0.8–12 keV). At least ten sources below our detection limit of $\approx 10^{29.2}$erg s^{-1} would be needed to account for this luminosity. The required source density of ≥ 10 sources per 80 arcmin^2 is easily accounted for by the known infrared population (cf. Greene, Young 1992). A hard excess similar to that seen here with $kT \approx 5$ keV has also been detected by Ginga in the Orion star-forming region (Yamauchi, Koyama 1993).

© Astronomical Society of Japan • Provided by the NASA Astrophysics Data System

1994PASJ...46L.125K

The data for DoAr 21 show that impulsive flare-like variability is not a necessary condition for hard X-ray emission from T Tauri stars. Its light curve is remarkably steady down to a time resolution of $\approx$ 4min, with a variability probability $\leq$ 1 %. This raises questions as to whether the standard intepretation of X-ray emission from T Tauri stars in terms of scaled-up solar-like activity is appropriate for DoAr 21. However, the hard emission of sources 8 and 10 is accompanied by variability, and the solar analogy may be appropriate for these two objects. As already noted, the variability of source 8 is flare-like, but the variability of source10 is qualitatively different. Its light curve shows a longer-term decline on a timescale of $\approx$ 8 hours with a peak-to-trough ratio of $\approx$ 3. This type of slower variability is much more suggestive of rotational effects such as spot modulation than of impulsive energy release from a flare.

Because of its brightness, we examined the GIS and SIS spectra of DoAr 21 in detail. Even so, it is not an ideal candidate for spectral analysis since it is located off-axis near the edge of the CCD and there are other sources within 3′ that can be seen in ROSAT images. We thus restricted the circular region used to extract the spectra to a radius of 1′.3. For the higher resolution SIS 0/1 spectra (figure 3), two-temperature RS models give $kT_1 = 0.4$–0.6 keV, $kT_2 = 1.55$–2.1 keV, and $\log N_{\rm H} = 22.30{\rm cm}^{-2}$. Similar fits of the GIS spectra favor the higher temperatures. Both SIS spectra show a possible weak line from S XIV/XV at 2.46 keV. Because the line emission is weak overall, we were able to obtain equally good fits to the SIS spectra with a single temperature TB model of $kT = 1.6$ keV and $\log N_{\rm H} = 22.04{\rm cm}^{-2}$. The range in column densities derived from these different fits implies a visual extinction of $A_V \approx 5$–8 magnitudes, which is consistent with the value $A_V = 6.6$ obtained from optical studies (Bouvier, Appenzeller 1992).

We thank the ASCA operations, instrument development, and software teams who have made this study possible.

References

Bouvier J., Appenzeller I. 1992, A&AS 92, 481
Burke B.E., Mountain R.W., Harrison D.C., Bautz M.W., Doty J.P., Ricker G.R., Daniels P.J. 1991, IEEE Trans. ED-38, 1069
de Geus E.J., Burton W.B. 1991, A& A 246, 559
Feigelson E.D., Giampapa M.S., Vrba F.J. 1991, in The Sun in Time, ed C.P. Sonett, M.S. Giampapa, M.S. Matthews (University of Arizona, Tucson) p658
Gorenstein P.,1975, ApJ 198, 95
Grasdalen G.L., Strom K.M., Strom S.E. 1973, ApJL 184, L53
Greene T.P., Young E.T. 1992, ApJ 395, 516
Herbig G.H., Bell K.R. 1988, Third Catalog of Emission-Line Stars of the Orion Population, Lick Obs. Bull. 1111
Koyama K., Asaoka I., Kuriyama T., Tawara Y. 1992, PASJ 44, L255
Montmerle T., Koch-Miramond L., Falgarone E., Grindlay J.E. 1983, ApJ 269, 182
Ohashi T., Makishima K., Ishida M., Tsuru T., Tashiro M., Mihara T., Kohmura Y., Inoue H. 1991, Proc SPIE 1549, 9
Serlemitsos J.P., Jalota L., Soong Y., Kunieda H., Tawara Y., Tsusaka Y., Suzuki H., Sakima Y. et al. 1944, PASJ submitted
Strom K.M., Strom S.E. 1994, ApJ in press
Struve O., Rudkjøbing M. 1949, ApJ 109, 92
Tanaka Y., Inoue H., Holt S.S. 1994 PASJ 46, L37
Vrba F.J., Strom S.E., Strom K.M. 1976, AJ 81, 958
Wilking B.A., Lada C.J. 1983, ApJ 274, 698
Yamauchi S., Koyama K. 1993, ApJ 405, 268

© Astronomical Society of Japan • Provided by the NASA Astrophysics Data System

1994PASJ...46L.125K

© Astronomical Society of Japan • Provided by the NASA Astrophysics Data System